

# How are galaxies assigned to halos?

## Searching for assembly bias in the SDSS galaxy clustering

Mohammadjavad Vakili<sup>1</sup>, Chang Hoon Hahn<sup>1</sup>

mjvakili@nyu.edu

### ABSTRACT

Clustering of dark matter halos has been shown to depend on halo properties beyond mass such as halo concentration, a phenomenon referred to as halo assembly bias. Standard halo occupation modeling (HOD) in large scale structure studies assumes that halo mass alone is sufficient in characterizing the connection between galaxies and halos. Modeling of galaxy clustering can face systematic effects if the number of galaxies are correlated with other halo properties. Using the Small MultiDark-Planck high resolution  $N$ -body simulation and the measurements of the projected two-point correlation function and the number density of Sloan Digital Sky Survey (SDSS) DR7 main galaxy sample, we investigate the extent to which the dependence of halo occupation on halo concentration can be constrained, and to what extent allowing for this dependence can improve our modeling of galaxy clustering.

Given the SDSS clustering data, our constraints on HOD with assembly bias, suggests that satellite population is not correlated with halo concentration at fixed halo mass. Furthermore, in terms of the occupation of centrals at fixed halo mass, our results favor lack of correlation with halo concentration in the most luminous samples ( $M_r < -21.5, -21$ ), modest levels of correlation for  $M_r < -20.5, -20, -19.5$  samples, lack of correlation for  $M_r < -19, -18.5$  samples, and anti-correlation for the faintest sample  $M_r < -18$ .

We show that in comparison with abundance-matching mock catalogs, our findings suggest qualitatively similar but modest levels of the impact of halo assembly bias on galaxy clustering. That is, the effect is only present in the central occupation and becomes less significant in brighter galaxy samples. Furthermore, by performing model comparison based on information criteria, we find that in most cases, the standard mass-only HOD model is still favored by the observations.

---

<sup>1</sup>Center for Cosmology and Particle Physics, Department of Physics, New York University, 4 Washington Pl, New York, NY, 10003

*Subject headings:* Cosmology: large-scale-structure of the universe, galaxies: halos

## 1. Introduction

Most theories of cosmology and large-scale structure formation under consideration today rely on the central assumption that galaxies reside in dark matter halos. Detailed study of the galaxy–halo connection is therefore critical in order to constrain cosmological models (by modeling galaxy clustering at non-linear scales) as well as providing a window into galaxy formation physics. One of the most powerful methods for describing the galaxy–halo connection is the halo occupation distribution (HOD, see [Seljak 2000](#); [Berlind & Weinberg 2002](#); [Scoccimarro et al. 2001](#); [Zheng et al. 2005, 2007](#); [Leauthaud et al. 2012](#); [Tinker et al. 2013](#); [Hearin et al. 2016b](#); [Hahn et al. 2016](#)).

HOD is an empirical framework that provides an analytic prescription for the expected number of galaxies  $N$  that reside in halos by specifying a probability distribution function  $P(N|x)$  where  $x$  is a property of the halo. The assumption of the standard HOD modeling is that the halo mass  $M$  alone is sufficient in determining the galaxy population of a halo. That is, the statistical properties of galaxies is governed by the halo mass. Mathematically, this assumption can be written as  $P(N|M, \{x\}) = P(N|M)$  where  $\{x\}$  is the set of all possible halo properties beyond halo mass  $M$ .

Despite this simplifying assumption, the models of galaxy–halo connection based on HOD have been successfully used in fitting the measurements of a wide range of statistics such as the projected two-point correlation function of galaxies, small scale redshift space distortion, three-point function, and galaxy–galaxy lensing with remarkable success (e.g. [Zheng et al. 2007](#); [Tinker 2007](#); [Zehavi et al. 2011](#); [Leauthaud et al. 2012](#); [Parejko et al. 2013](#); [Coupon et al. 2015](#); [Guo et al. 2015a,b](#); [Miyatake et al. 2015](#); [Zu & Mandelbaum 2015](#); [Guo et al. 2016](#)). HOD has been used in constraining the cosmological parameters through modeling the galaxy two-point correlation function (hereafter 2PCF) ([Abazajian et al. 2005](#)), combination of 2PCF with mass-to-light ratio of galaxies ([Tinker et al. 2005](#)), redshift space distortions ([Tinker 2007](#)), mass-to-number ratio of galaxy clusters ([Tinker et al. 2012](#)) galaxy-galaxy weak lensing ([van den Bosch et al. 2003](#); [Cacciato et al. 2013](#); [More et al. 2013](#); [van den Bosch et al. 2013](#)) in the main sample of galaxies of the Sloan Digital Sky Survey (hereafter SDSS, [York et al. 2000](#)), and also the combination of galaxy clustering and galaxy-galaxy lensing ([More et al. 2015](#)) in SDSS III Baryon Oscillation Spectroscopic Survey (BOSS, [Dawson et al. 2013](#)). Furthermore, HOD is implemented in producing mock galaxy catalogs in the BOSS survey ([Manera et al. 2013](#); [White et al. 2014](#)). It has also been

used in galaxy evolution studies (Conroy & Wechsler 2009; Leauthaud et al. 2012; Behroozi et al. 2013a; Hudson et al. 2015; Zu & Mandelbaum 2015, 2016).

The complexity of structure formation however, is not sufficiently modeled under the standard HOD framework. Numerous  $N$ -body simulations that examine the clustering of dark matter halos have demonstrated that halo clustering is correlated with the formation history of halos. That is, at a fixed halo mass, the halo bias is correlated with properties of halos beyond mass, such as the concentration, formation time, or etc. This phenomenon is known as halo assembly bias (see Sheth & Tormen 2004; Gao et al. 2005; Harker et al. 2006; Wechsler et al. 2006; Gao & White 2007; Croton et al. 2007; Wang et al. 2007; Angulo et al. 2008; Dalal et al. 2008; Li et al. 2008; Sunayama et al. 2016). It has been claimed that there is support for halo assembly bias in observations of SDSS redMaPPer galaxy clusters (Miyatake et al. 2016).

Furthermore, the halo occupation may also depend on the formation history of halos. Then we may expect the spatial statistics of galaxies to be tied to the halo properties beyond mass such as the concentration of halos. There have been many attempts in the literature at examining the dependence of halo occupation on environment of the halos. But the results are mixed, and there is very little consensus. Tinker & Conroy (2009) show that the properties of the galaxies that reside in voids can be explained by the halo mass in which they live, and their properties are independent of their large scale environment of the halos. Tinker et al. (2006) proposes an extension of the standard HOD model  $P(N|M)$  such that the number of galaxies residing in a halo not only depends on the mass of the halo, but also on the large scale density contrast  $P(N|M, \delta)$ . Based on modeling the clustering and void statistics of the SDSS galaxies, Tinker et al. (2008b) shows that the dependence of the expected number of central galaxies on large scale density is not very strong. By randomly shuffling the galaxies among host halos of similar mass in the Millenium simulation, Croton et al. (2007) shows that assembly bias significantly impacts the galaxy two-point correlation functions. They also show that the effect is different for the faint and the bright samples.

Another family of empirical galaxy–halo connection models is *Abundance Matching*. In Abundance Matching models, galaxies are assumed to live in halos and are assigned luminosities or stellar masses by assuming a monotonic mapping. In this monotonic mapping, the abundance of the halos are matched to the abundance of some property of galaxies (Kravtsov et al. 2004; Vale & Ostriker 2004; Tasitsiomi et al. 2004; Conroy & Wechsler 2009; Guo et al. 2010; Wetzel & White 2010; Neistein et al. 2011; Watson et al. 2012; Rodríguez-Puebla et al. 2012; Kravtsov 2013; Mao et al. 2015; Chaves-Montero et al. 2016). One of the most commonly used host halo properties in abundance matching is the maximum circular velocity of the host halo  $V_{\text{max}}$  that traces the depth of the gravitational potential well of

the halo. Furthermore, a scatter is assumed in this mapping. Within this galaxy–halo connection framework, abundance matching models have been successfully used in modeling a wide range of the statistical properties of galaxies such as two-point correlation function (Reddick et al. 2013; Lehmann et al. 2015; Guo et al. 2016) as well as the group statistics of galaxies (Hearin et al. 2013).

It has been shown that the abundance matching mock catalogs that use  $V_{\text{max}}$  (see Hearin & Watson 2013; Zentner et al. 2014), or the ones that use some combination of  $V_{\text{max}}$  and host halo virial mass  $M_{\text{vir}}$  (see Lehmann et al. 2015) exhibit significant levels of assembly bias. That is, halo occupation in these models depends not only on halo mass, but also on other halo properties. This has been demonstrated by randomizing the galaxies among host halos in bins of halo mass, such that the HOD remains constant, and then comparing the difference in the 2PCF of the randomized catalog and that of the original mock catalog.

Based on the projected 2PCF measurements of (Hearin & Watson 2013) galaxy catalogs, Zentner et al. (2014) showed that after fitting the 2PCF measurements of these catalogs with the standard *mass-only* HOD modeling, the inferred HOD does not match the *true* halo occupation of these catalogs. That is, in the presence of assembly bias in a galaxy sample, one can fit the clustering of this sample with the standard *mass-only* HOD, but that does not guarantee recovery of the true HOD parameters.

In this work, we aim to investigate the dependence of halo occupation on halo concentration, and how this dependence can be constrained in the low-redshift universe with the measurements of the 2PCF of galaxies with a wide range of luminosities in the SDSS DR7 main galaxy sample. In order to achieve this goal, we need to adopt a HOD model that takes into account a dependence on halo properties beyond mass. There are a number of frameworks in the literature. Tinker et al. (2008b); Gil-Marín et al. (2011); McEwen & Weinberg (2016) have proposed environment-dependent HOD modeling methods that take into account the large-scale density contrast. The model that we use in this investigation is the decorated HOD framework (Hearin et al. 2016b). In the decorated HOD framework, at a fixed halo mass, halos are populated with galaxies according to the standard HOD modeling. Then, a secondary halo property is selected. At a fixed halo mass, halos are split into two populations: halos with the highest and halos with the lowest values of the secondary property. The two population receive enhancements (decrements) in their number of galaxies according to a assembly bias amplitude parameter. The assembly bias parameter will not be degenerate with the rest of the HOD parameters.

The advantage of this framework is that the more complex HOD model is identical to the underlying *mass-only* HOD model in every respect, except that at a fixed halo mass, halos receive enhancement (decrements) in the number of galaxies they host according to the

value of their secondary property. In order to constrain assembly bias along with the rest of the HOD parameters, we make use of the publicly available measurements of the projected 2PCF and number density measurements made by (Guo et al. 2015b). These measurements made use of the NYU Value-Added Galaxy Catalog (Blanton et al. 2005).

Furthermore, we discuss how taking assembly bias into account in a more complex HOD model can improve our modeling of galaxy clustering in certain brightness limits. Then, we make a qualitative comparison between the levels of the impact of assembly bias in our best-fit decorated HOD model on galaxy clustering, and the impact of assembly bias present in (Hearin & Watson 2013) catalogs on galaxy clustering. Our comparison shows the levels of the impact of assembly bias on galaxy clustering seen in the predictions of both models follow the same trend. That is assembly bias is more prominent in lower luminosity-threshold samples and its impact on galaxy clustering is only significant on large scales (more than a few Mpc).

In order to investigate whether the additional complexity of the decorated HOD model is demanded by the galaxy clustering data, we perform a model comparison between the standard HOD model and the HOD model with assembly bias. We also discuss the effect of our choice of  $N$ -body simulation on our constraints, and previous works in the literature (Zentner et al. 2016) based on smaller  $N$ -body simulations. In addition to analysis of the luminosity-threshold samples presented in Zentner et al. (2016), we consider the faintest ( $M_r < -18, -18.5$ ) and the brightest ( $M_r < -20.5$ ) galaxy samples. For the samples considered in both Zentner et al. (2016) and this investigation, we compare the constraints on the expected levels of assembly bias.

This paper is structured as follows: In Section 2 we discuss the  $N$ -body simulation, the two halo occupation modeling methods, and the details of the computation of model observables used in this investigation. Then in Section 3, we discuss the data used in this study. In Section 4 we discuss the details of our inference analysis as well as the results. This includes description of the details of our inference setup. In Section 5 we discuss the constraints and their implications. This includes presentation of the constraints on the parameters of the two models, interpretation of the predictions of our constraints and their possible physical ramifications, assessment of the levels of assembly bias as predicted by our model constraints and its comparison with abundance matching mock catalogs, and finally model comparison. Finally, we discuss and conclude in Section 6. Throughout this paper, unless stated otherwise, all radii and densities are stated in comoving units. Standard flat  $\Lambda$ CDM is assumed, and all cosmological parameters are set to the Planck 2015 best-fit estimates.

## 2. Method

In this section, we discuss the ingredients of our modeling one-by-one. First, we discuss the simulation used in this study. Afterwards, we talk about the forward modeling of galaxy catalogs in the standard HOD modeling framework as well as the decorated HOD framework. Then, we provide an overview of the two summary statistics of the galaxy catalogs that we used in our inference.

### 2.1. Simulation

For the simulations used in this work, we make use of the Rockstar (Behroozi et al. 2013b) halo catalogs in the  $z = 0$  snapshot of the Small MultiDark of Planck cosmology (referred to as SMDP) (Klypin et al. 2016). This high resolution  $N$ -body simulation (publicly available at <https://www.cosmosim.org>) was carried out using the GADGET-2 code (see Klypin et al. 2016 and references therein) code, following the Planck  $\Lambda$ CDM cosmological parameters  $\Omega_m = 0.307$ ,  $\Omega_b = 0.048$ ,  $\Omega_\Lambda = 0.693$ ,  $\sigma_8 = 0.823$ ,  $n_s = 0.96$ ,  $h = 0.678$ . The Box size for this  $N$ -body simulation is  $0.4 h^{-1}\text{Gpc}$ , the number of simulation particles is  $3840^3$ , the mass per simulation particle  $m_p$  is  $9.6 \times 10^7 h^{-1}M_\odot$ , and the gravitational softening length  $\epsilon$  is  $1.5 h^{-1}\text{kpc}$ .

In the SMDP simulation, as discussed in Rodríguez-Puebla et al. (2016), the Rockstar algorithm can reliably resolve halos with  $\geq 100$  particles which corresponds to  $M_{\text{vir}} \geq 9.6 \times 10^9 h^{-1}M_\odot$ . The advantage of using the SMDP simulation is that it satisfies both the size and resolution requirements of studying the galaxy–halo connection in a wide range of luminosity thresholds. Fainter galaxy samples reside in lower mass halos, and the more luminous galaxy samples considered in this investigation occupy higher comoving volumes. Furthermore, since we are studying the higher order halo occupation statistics, the concentration-dependence in particular, it is important to use a simulation that can resolve the internal structure of halos. In the context of Subhalo-Abundance matching modeling, accuracy of which depends on subhalo completeness especially in the low mass limit, the SMDP simulation has been used to model the faintest galaxy samples in the SDSS data (see Guo et al. (2016)). The added advantage of using the SMDP simulation over some of the other industrial simulation boxes commonly used in the literature such as Bolshoi (Klypin et al. 2011, 2016) simulation is its larger comoving volume. Larger volume makes this simulation more suitable for performing inference with  $L_\star$  (corresponding to  $M_r \sim -20.44$ , see Blanton et al. 2003) and more luminous than  $L_\star$  galaxy samples that occupy larger comoving volumes.

## 2.2. Halo occupation modeling

### 2.2.1. standard model without assembly bias

For our standard HOD model, we assume the HOD parameterization from [Zheng et al. \(2007\)](#). According to this model, a dark matter halo can host a central galaxy and some number of satellite galaxies. The occupation of the central galaxies follows a nearest-integer distribution, and the occupation of the satellite galaxies follows a Poisson distribution. The expected number of centrals and satellites as a function of the host halo mass of  $M_h$  are given by the following equations

$$\langle N_c | M_h \rangle = \frac{1}{2} \left[ 1 + \left( \frac{\log M_h - \log M_{\min}}{\sigma_{\log M}} \right) \right], \quad (1)$$

$$\langle N_s | M_h \rangle = \left( \frac{M_h - M_0}{M_1} \right)^\alpha. \quad (2)$$

For populating the halos with galaxies, we follow the procedure described in [Hahn et al. \(2016\)](#), and [Hearin et al. \(2016b\)](#). The central galaxies are assumed to be at the center of the host dark matter halos. We assume that the central galaxies are at rest with respect to the bulk motion of the halos and their velocities are given by the velocity of the center of mass of their host halo. Note that this assumption is shown to be violated in brighter than  $L_*$  galaxy samples (see [Guo et al. 2015b](#)). But since we are not considering the redshift space 2PCF multipoles in our study, we do not expect this velocity bias to impact our inference. We place the satellite galaxies within the virial radius of the halo following a Navarro-Frenk-White profile (hereafter NFW; [Navarro et al. 2004](#)). This approach is different from other simulation-based halo occupation modeling techniques (see [Guo et al. 2016](#); [Zheng & Guo 2016](#)) in that the positions of the satellites are not assigned to the dark matter particles in the  $N$ -body simulation. The concentration of the NFW profile is given by the empirical mass-concentration relation provided by [Dutton & Macciò \(2014\)](#). The velocities of the satellite galaxies are given by two components. The first component is the velocity of the host halo. The second component is the velocity of the satellite galaxy with respect to the host halo which is computed following the solution to the NFW profile Jeans equations ([More et al. 2009](#)). We refer the readers to [Hearin et al. \(2016b\)](#) for a more comprehensive and detailed discussion of the forward modeling of the galaxy mock catalogs.

### 2.2.2. Model with Assembly bias

Now let us provide a brief overview of HOD modeling with **Heaviside Assemblybias** (referred to as the decorated HOD) introduced in [Hearin et al. \(2016b\)](#). At a fixed halo



mass  $M_h$ , halos are split into two populations: population of halos with the 0.5-percentile of highest concentration, and population of halos with 0.5 percentile of lowest concentration. For simplicity, we call the first population “type-1” halos, and the second population “type-2” halos. In the decorated HOD model, the expected number of central and satellite galaxies at a fixed halo mass  $M_h$  in the two populations are given by

$$\langle N_{c,i} | M_h, c \rangle = \langle N_c | M_h \rangle + \Delta N_{c,i}, \quad i = 1, 2 \quad (3)$$

$$\langle N_{s,i} | M_h, c \rangle = \langle N_s | M_h \rangle + \Delta N_{s,i}, \quad i = 1, 2 \quad (4)$$

where  $\langle N_c | M_h \rangle$  and  $\langle N_s | M_h \rangle$  are given by Eqs 1 and 2 respectively, and we have  $\Delta N_{s,1} + \Delta N_{s,2} = 0$ , and  $\Delta N_{c,1} + \Delta N_{c,2} = 0$ . These two conditions ensure the conservation of HOD. At a given host halo mass  $M_h$ , the central occupation of the the two populations follows a nearest-integer distribution with the first moment given by 3; and the satellite occupation of the the two populations follows a Poisson distribution with the first moment given by 4.

In this occupation model, the allowable ranges that quantities  $\Delta N_{c,1}$  and  $\Delta N_{s,1}$  can take are given by

$$\max\{-\langle N_c | M_h \rangle, \langle N_c | M_h \rangle - 1\} \leq \Delta N_{c,i} \leq \min\{\langle N_c | M_h \rangle, 1 - \langle N_c | M_h \rangle\}, \quad (5)$$

$$-\langle N_s | M_h \rangle \leq \Delta N_{s,i} \leq \langle N_s | M_h \rangle. \quad (6)$$

Afterwards, the assembly bias parameter  $\mathcal{A}$  is defined in the following way:

$$\Delta N_{\alpha,1}(M_h) = |\mathcal{A}_\alpha| \Delta N_{\alpha,1}^{\max}(M_h) \quad \text{if } \mathcal{A}_\alpha > 0, \quad (7)$$

$$\Delta N_{\alpha,1}(M_h) = |\mathcal{A}_\alpha| \Delta N_{\alpha,1}^{\min}(M_h) \quad \text{if } \mathcal{A}_\alpha < 0, \quad (8)$$

where the subscript  $\alpha = c, s$  stands for the centrals and satellites respectively, and  $\Delta N_{\alpha,1}^{\max}(M_h)$ ,  $\Delta N_{\alpha,1}^{\min}(M_h)$  are given by Eqs. 5 and 6.

For a given  $\mathcal{A}_\alpha$ , once  $\Delta N_{\alpha,1}$  is computed using equation (7)—if  $\mathcal{A}_\alpha > 0$ —or equation (8)—if  $\mathcal{A}_\alpha < 0$ —,  $\Delta N_{\alpha,2} = 1 - \Delta N_{\alpha,1}$  is computed. At a fixed halo mass  $M_h$ , once the first moments of occupation statistics for the *type-1* and *type-2* halos are determined, we perform the same procedure described in 2.2.1 to populate the halos with mock galaxies.

### 2.2.3. Redshift-space distortion

Once the halo catalogs are populated with galaxies, the real-space positions and velocities of all mock galaxies are obtained. The next step is applying a redshift-space distortion



transformation by assuming plane-parallel approximation. Our use of plane parallel approximation is justified because of the narrow redshift range of the SDSS main galaxy sample considered in this study. If we assume that the  $\hat{z}$  axis is the line-of-sight direction, then with the transformation  $(X, Y, Z) \rightarrow (S_x, S_y, S_z) = (X, Y, Z + v_z(1 + z)/H(z))$  for each galaxy with the real space coordinates  $(X, Y, Z)$ , velocities  $(v_x, v_y, v_z)$ , and redshift  $z$ , we obtain the redshift-space coordinate of the produced mock galaxies. Here we assume  $z \simeq 0$ , and therefore transformation is given by  $(X, Y, Z) \rightarrow (X, Y, Z + v_z/H_0)$ .

### 2.3. Model Observables

As described in [Hearin et al. \(2016b\)](#) and [Hahn et al. \(2016\)](#), this approach makes no appeal to the fitting functions used in the analytical calculation of the 2PCF. The accuracy of these fitting functions is limited ([Tinker et al. 2008a, 2010](#); [Watson et al. 2013](#)). Our approach also does not face the known issues of the treatment of halo exclusion and scale-dependent bias that can lead to potential inaccuracies in halo occupation modeling (see [van den Bosch et al. 2013](#)).

The projected 2PCF  $w_p(r_p)$  can be computed by integrating the 3D redshift space 2PCF  $\xi(r_p, \pi)$  along the line-of-sight (where  $r_p$  and  $\pi$  denote the projected and line-of-sight separation of galaxy pairs respectively):

$$w_p(r_p) = 2 \int_0^{\pi_{max}} \xi(r_p, \pi) d\pi \quad (9)$$

For our 2PCF calculations, we use the  $w_p$  measurement functionality of the fast and publicly available pair-counter code **CorrFunc** ([Sinha 2016](#), available at <https://github.com/manodeep/Corrfunc>). To be consistent with the SDSS measurements described in Section 3,  $w_p(r_p)$  is obtained by the line-of-sight integration to  $\pi_{max} = 40 h^{-1}\text{Mpc}$ . Note that  $w_p(r_p)$  is measured in units of  $h^{-1}\text{Mpc}$ . To be consistent with [Guo et al. \(2015b\)](#), we use the same binning (as specified in Section 3) to measure  $w_p$ . In addition to the projected 2PCF, we use the number density given by the number of mock galaxies divided by the comoving volume of the **SMDP** simulation.

Note that a full forward model of the data requires running the simulation at different redshifts, generation of light cones, accounting for the complex survey geometry and systematic errors such as fiber collisions. Using the  $z = 0$  output of the **SMDP** simulation in our forward model of the spatial distribution of galaxies is only an approximation. This approximation can be justified by the small redshift range of the SDSS DR7 main galaxy sample. As described in [Zehavi et al. 2011](#), using random catalogs with angular window function of

the data in measurements of galaxy clustering accounts for the geometry of the data. As described in Section 3, the fiber collision correction method of Guo et al. 2012 is applied to the SDSS clustering measurements used in this study. Therefore we do not account for that effect in our forward model.

### 3. Data

We focus on the measurements made on the volume-limited luminosity-threshold main sample of galaxies in the SDSS spectroscopic survey. In this section, we briefly describe the measurements used in our study for finding constraints on the assembly bias as well as the HOD parameters.

The measurements consist of the number density  $n_g$  and the projected 2PCF  $w_p(r_p)$  made by Guo et al. (2015b) for the volume-limited sample of galaxies in NYU Value Added Galaxy Catalog (Blanton et al. 2005) constructed from the SDSS DR7 main galaxy sample (Abazajian et al. 2009). In particular, eight volume-limited luminosity-threshold samples are constructed with maximum absolute luminosity in  $r$ -band of -18, 18.5, -19, -19.5, -20, -20.5, -21, and -21.5. Qualitatively, these samples are constructed in a similar way to those constructed in Zehavi et al. (2011). For detailed differences between the samples in Guo et al. (2015b) and Zehavi et al. (2011), we refer the reader to the Table 1 and Table 2 in those papers respectively.

The projected 2PCFs are measured in 12 logarithmic  $r_p$  bins (in units of  $h^{-1}\text{Mpc}$ ) of width  $\Delta \log(r_p) = 0.2$ , starting from  $r_p = 0.1 h^{-1}\text{Mpc}$ . For all luminosity threshold samples, the integration along the line-of-sight (9) are performed to  $\pi_{max} = 40 h^{-1}\text{Mpc}$ .

The 2PCF measurement of each luminosity-threshold sample is accompanied by a covariance matrix constructed using 400 jackknife sub-samples of the data. The number density measurements are also accompanied by uncertainties measured using the jackknife method. Furthermore, the covariance between the number density and the projected 2PCF measurements are neglected. As Norberg et al. (2009) shows, parameter estimation using jackknife covariance matrices is conservative as the jackknife method overestimates the errors in the observations.

The advantage of using these measurements is that the effects of fiber collision systematic errors on the two-point statistics are corrected for (with the method described in Guo et al. 2012), and therefore, these measurements provide accurate small scale clustering measurements. The assembly bias parameters introduced in section 2 can have a 10-percent level impacts on galaxy clustering (Hearin et al. 2016b). Presence of assembly bias in the

satellite population impacts the very small-scale clustering (Hearin et al. 2016b). Moreover as Sunayama et al. (2016) demonstrates, the scale-dependence of the halo assembly bias has a pronounced bump in the 1-halo to 2-halo transition regime ( $1 \sim 2 h^{-1}\text{Mpc}$ ). This scale can be impacted by fiber collision systematics. Precise investigation of the possible impact of this signal on the galaxy clustering modeling requires accurate measurements of 2PCF on small scales. The method of Guo et al. (2012) is able to recover the true  $w_p$  with  $\sim 6\%$  accuracy in small scales ( $r_p = 0.1 h^{-1}\text{Mpc}$ ) and with  $\sim 2.5\%$  at relatively large scales  $r_p \sim 30 h^{-1}\text{Mpc}$ .

Note that the comoving volume of the  $N$ -body simulation used in this investigation is  $64 \times 10^6 h^{-3}\text{Mpc}^3$  which is larger than the comoving volume of all the luminosity-threshold samples in the SDSS data considered in this study except the two most luminous samples. The comoving volumes of the  $M_r < -21$ ,  $21.5$  samples are 71.74 and 134.65 (in units of  $10^6 h^{-3}\text{Mpc}^3$ ) respectively. Since we are not studying very large scale clustering ( $r_{p, \max} \leq 25 h^{-1}\text{Mpc}$ ), using a slightly smaller box for those samples is justified.

## 4. Analysis

### 4.1. Inference setup

Given the SDSS measurements described in Section 3, we aim to constrain the HOD model without assembly bias (described in 2.2.1), and the HOD model with assembly bias (described in 2.2.2) for each luminosity-threshold sample, by sampling from the posterior probability distribution  $p(\theta|d) \propto p(d|\theta)\pi(\theta)$  where  $\theta$  denotes the parameter vector and  $d$  denotes the data vector. In the standard HOD modeling  $\theta$  is given by

$$\theta = \{\log M_{\min}, \sigma_{\log M}, \log M_0, \alpha, \log M_1\}, \quad (10)$$

and in the HOD modeling with assembly bias we have

$$\theta = \{\log M_{\min}, \sigma_{\log M}, \log M_0, \alpha, \log M_1, \mathcal{A}_{\text{cen}}, \mathcal{A}_{\text{sat}}\}, \quad (11)$$

Furthermore, data (denoted by  $d$ ) is the combination of  $[n_g, w_p(r_p)]$ . The negative log-likelihood (assuming negligible covariance between  $n_g$  and  $w_p(r_p)$ ) is given by

$$-2 \ln p(d|\theta) = \frac{[n_g^{\text{data}} - n_g^{\text{model}}]^2}{\sigma_n^2} + \Delta w_p^T \widehat{C}^{-1} \Delta w_p + \text{const.}, \quad (12)$$

where  $\Delta w_p$  is a 12 dimensional vector,  $\Delta w_p(r_p) = w_p^{\text{data}}(r_p) - w_p^{\text{model}}(r_p)$ , and  $\widehat{C}^{-1}$  is the estimate of the inverse covariance matrix that is related to the inverse of the jackknife

covariance matrix (provided by Guo et al. 2015b)  $\widehat{C}^{-1}$ , following Hartlap et al. (2007):

$$\widehat{C}^{-1} = \frac{N - d - 2}{N - 1} \widehat{C}^{-1}, \quad (13)$$

where  $N = 400$  is the number of the jackknife samples, and  $d = 12$  is the length of the data vector  $w_p$ . Another important ingredient of our analysis is specification of the prior probabilities  $\pi(\theta)$  over the parameters of the halo occupation models considered in this study. For both models, we use uniform flat priors for all the parameters. The prior ranges are specified in the Table 4.1. Note that a uniform prior between -1 and 1 is chosen for assembly bias parameters since these parameters are, by definition, bounded between -1 and 1.

For sampling from the posterior probability, given the likelihood function (see equation 12) and the prior probability distributions (see Table 4.1), we use the affine-invariant ensemble MCMC sampler (Goodman & Weare 2010) and its implementation `emcee` (Foreman-Mackey et al. 2013). In particular, we run the `emcee` code with 20 walkers and we run the chains for at least 10000 iterations. We discard the first one-third part of the chains as burn-in samples and use the reminder of the chains as production MCMC chains. Furthermore, we perform Gelman-Rubin convergence test (Gelman & Rubin 1992) to ensure that the MCMC chains have reached convergence.

## 5. Results and Discussion

### 5.1. constraints and interpretations

Our constraints on the assembly bias parameters fall into two main categories. First, the satellite assembly bias parameter  $\mathcal{A}_{\text{sat}}$  and the second, the central assembly bias parameter  $\mathcal{A}_{\text{cen}}$ . As shown in Figure 1, for all the eight luminosity-threshold samples in the SDSS DR7 data, our constraints on the parameter  $\mathcal{A}_{\text{sat}}$  are consistent with zero. On the other hand, our constraints on the parameter  $\mathcal{A}_{\text{cen}}$ —albeit not tightly constrained—show a trend which can be summarized as the following. In the most luminous galaxy samples, i.e.  $M_r < -21.5$  and  $M_r < -21$ ,  $\mathcal{A}_{\text{cen}}$  is poorly constrained and the constraints are equivalent to zero. As we investigate less luminous samples,  $M_r < -20.5, -20, -19.5$ , our constraints on  $\mathcal{A}_{\text{cen}}$  shift toward positive values, with the  $M_r < -20$  sample favoring the highest values for  $\mathcal{A}_{\text{cen}}$ . Furthermore, the posterior constraints on the assembly bias parameters in the slightly fainter samples, i.e.  $M_r < -19$  and i.e.  $M_r < -18.5$ , are consistent with zero. In the faintest galaxy sample, i.e.  $M_r < -18$ , our constraints favor negative values of  $\mathcal{A}_{\text{cen}}$ .

The underlying theoretical consideration for explaining the assembly bias of the central

and satellite galaxies are different. The large scale clustering—or the two halo term in the galaxy clustering—is mainly governed by the clustering of the central galaxies. The central galaxy clustering can be thought as the weighted average over the halo clustering. The large scale bias of the dark matter halo clustering depends not only on mass, but also on the other properties of halos beyond mass, such as concentration (Wechsler et al. 2006; Gao & White 2007; Miyatake et al. 2016), spin (Gao & White 2007), formation time (Gao & White 2007; Li et al. 2008), and maximum circular velocity of the halo  $V_{\max}$  (Sunayama et al. 2016).

In particular, findings of Wechsler et al. (2006) and Sunayama et al. (2016) have demonstrated that for halos with mass bellow the collapse mass ( $M \leq M_{\text{col}} \simeq 10^{12.5} M_{\odot}$ ) the large scale bias of high- $V_{\max}$  (or equivalently high- $c$  halos at a fixed halo mass) is larger than that of the low- $V_{\max}$  (low- $c$  halos). This signal reverses and weakens for the high mass halos ( $M \geq M_{\text{col}}$ ). Note that the halo concentration traces the maximum circular velocity  $V_{\max}$  such that halos with higher  $V_{\max}$  have higher concentration and vice versa (see Prada et al. 2012). For halos described by NFW profile, at a fixed halo mass, halos with higher values of concentration have higher values of  $V_{\max}$ .

Furthermore, investigation of the scale dependence of halo assembly bias has shown that the ratio of the bias of high- $V_{\max}$  halos and the low- $V_{\max}$  halos has a bump-like feature in the quasi-linear scales  $\sim 0.5 \text{ Mpc} h^{-1} - 5 \text{ Mpc} h^{-1}$ . From the theoretical standpoint, this phenomenon has been attributed to a population of distinct halos with  $M \sim 10^{11.7} h^{-1} M_{\odot}$  at the present time that are close to the most massive groups and clusters (Sunayama et al. 2016, and see More et al. 2016 for the observational investigation of this signal by means of galaxy-galaxy lensing). The clustering of these population of halos is therefore dictated by that of the massive halos. Note that this scale-dependent bias feature vanishes in high mass halos.

Consequently, at a fixed halo mass less than  $M_{\text{col}}$ , assignment of more central galaxies to the high- $c$  halos (higher expected number of central galaxies in the high- $c$  halos) gives rise to a boost in the galaxy clustering in the linear scales as well as in regimes corresponding to the one-halo to two-halo transition. For the more massive halos ( $M \geq M_{\text{col}}$ ), we expect the large-scale clustering boost to reverse sign, and the quasi-linear bump feature to vanish.

Figure 2 demonstrates the 68% and 95% posterior predictions for the projected 2PCF  $w_p$  from the occupation model without assembly bias (shown in red) and the occupation model with assembly bias (shown in blue) for all eight luminosity-threshold samples. For the brightest galaxies,  $M_r < -21.5$  and  $M_r < -21.0$ , the posterior prediction of  $w_p$  from the two models are consistent with one another. Note that these galaxies reside in the most massive halos ( $M > M_{\text{col}}$ ) for which the scale-dependence of the halo assembly bias and the difference between the large-scale bias of the high- $c$  and low- $c$  halos become negligible.

Figure 3 shows the fractional difference between the 68% and 95% posterior predictions of  $w_p$  and the SDSS data. It is evident from Figure 3 that some improvement on modeling the clustering of the samples of  $L_\star$  and slightly less brighter than  $L_\star$  galaxies can be achieved by employing the more complex halo occupation model with assembly bias. As a result of apportioning more central galaxies to the high- $c$  halos relative to the low- $c$  halos, in the samples with luminosity thresholds of  $M_r < -20.5, -20, -19.5$ , the posterior predictions for  $w_p$  are slightly improved in the intermediate scales ( $1 \sim 2 \text{ Mpc}h^{-1}$ ) and large scales. This can be also noted in significantly lower  $\chi^2$  values—at the cost more model flexibility and higher degrees of freedom—achieved by the assembly bias model in these luminosity-threshold samples (see Table 5.1).

In the sample of galaxies with the luminosity threshold  $M_r < -19, -18.5$ , the constraints on  $\mathcal{A}_{\text{cen}}$  become consistent with zero with the tendency towards positive values for the  $M_r < -19$  sample and towards more negative values for the  $M_r < -18.5$  sample. As shown in Figures 2 and 3, for the  $M_r < -19$  ( $M_r < -18.5$ ) sample this results in slightly higher (lower) posterior predictions for  $w_p$  in the intermediate toward large scales. Overall, for these two samples, the assembly bias parameters remain largely unconstrained and the decorated HOD model does not yield better  $\chi^2$  values.

Finally, In the faintest sample ( $M_r < -18$ ), negative constraints on the parameter  $\mathcal{A}_{\text{cen}}$  results in higher expected number of centrals in the low- $c$  halos, which at a fixed halo mass, cluster less strongly. This affects both the large scale bias and the intermediate regimes as a result of the scale-dependent bump feature (see Figures 2 and 3). Furthermore, the model with assembly bias provides better fit to the SDSS data in this luminosity-threshold sample.

The luminosity dependent trend in the constraints on the central assembly bias for the six dimmest samples can be attributed to the fact that the halo concentration is highly correlated with the maximum circular velocity  $V_{\text{max}}$  which is a tracer of the potential well of dark matter halos (Prada et al. 2012). In a dark matter halo described by an NFW profile, the depth of the gravitational potential well of dark matter halos can be directly measured by the maximum circular velocity  $V_{\text{max}}$  (van den Bosch et al. 2014). In particular, the magnitude of the potential well at the center of an NFW halo—where the central galaxy is assumed to reside—scales as  $V_{\text{max}}^2$ . More specifically, we have:

$$\Phi(r = 0) = -\left(\frac{V_{\text{max}}}{0.465}\right)^2, \quad (14)$$

where  $\Phi(r = 0)$  is the central potential of an NFW profile. Note that  $V_{\text{max}}$  is also the quantity often used in the abundance matching technique in which the luminosity of galaxies is monotonically matched to  $V_{\text{max}}$  (see for example Reddick et al. 2013; Lehmann et al. 2015; Guo et al. 2016; Rodríguez-Puebla et al. 2016). The trend between the constraint on  $\mathcal{A}_{\text{cen}}$

and the luminosity threshold of the samples may suggest that at a *fixed halo mass*, the central galaxies in the dimmest samples ( $M_r < -18$ ,  $-18.5$ ) tend to reside in dark matter halos with shallower gravitational well. In brighter galaxy samples ( $M_{\text{max}} < -19$ ,  $-19.5$ ,  $-20$ ,  $-20.5$ ), at a *fixed halo mass*, the central galaxies have a tendency to reside in dark matter halos with deeper gravitational potential well.

The satellite assembly bias can only significantly alter the galaxy clustering at small-to-intermediate scales. Assigning more satellite galaxies to lower (or higher) concentration halos affects the one-halo term through increasing the satellite-satellite pair counts  $\langle N_s N_s \rangle$ . This results in boosting the small-scale clustering. But as pointed out by [Hearin et al. \(2016b\)](#), the amount by which small-scale clustering increases also depends on the sign of the central assembly bias parameter  $\mathcal{A}_{\text{cen}}$ . Formation history of the halos can lead to the dependence of the abundance of subhalos on halo concentration ([Zentner et al. 2005](#); [Mao et al. 2015](#)) at fixed halo mass, and since the occupation of the satellite galaxies is related to the abundance of subhalos, the satellite occupation may depend on halo concentration.

However, our results suggest that for all the luminosity-threshold samples considered in this study, the satellite assembly bias parameter is largely unconstrained and consistent with zero. We do not expect the galaxy clustering data to be a sufficient statistics for obtaining constraints on the satellite assembly bias. Group statistics probes the high mass end of the galaxy–halo connection and is sensitive to the parameters governing the satellite population (see [Hearin et al. 2013](#); [Hahn et al. 2016](#)). Therefore these measurements may shed some light on potential presence of assembly bias in satellite population.

It is important to note that the halo mass range in which the central assembly bias  $\mathcal{A}_{\text{cen}}$  affects the central galaxy population is the mass range in which the condition  $0 < \langle N_c | M \rangle < 1$  is met. Consequently, larger scatter parameter  $\sigma_{\log M}$  increases the dynamical mass range in which assembly bias affects the galaxy clustering. Note that in the luminosity regimes for which we obtain tighter constraints on  $\mathcal{A}_{\text{cen}}$ , the best-estimate values of the scatter parameter  $\sigma_{\log M}$  appear to be higher in the model with assembly bias. This is evident in [Figure 8](#). The model with assembly bias tends to push  $\sigma_{\log M}$  to higher values. This can be attributed to the tendency of this model to increase the effective dynamical mass range of central assembly bias.

As shown in [Table 5.1](#), in the HOD model with assembly bias, the constraints found on the scatter parameter are not tight. This is in keeping with the results of [Guo et al. \(2015b\)](#) which uses the same SDSS measurements and finds that the scatter parameter remains largely unconstrained when only  $n_g$  and  $w_p$  are used as observables. Note that scatter is better constrained for the most luminous galaxy samples (this is attributed to the steep dependence of the halo bias and halo mass function on halo mass in the high mass end). But



since these samples live in the most massive halos, we do not expect the tighter constraints on scatter to help us constrain the central assembly bias parameter. Guo et al. (2015b) shows that by employing additional measurements such as the monopole ( $\xi_0$ ), quadrupole ( $\xi_2$ ), and hexadecapole ( $\xi_4$ ), one can obtain tighter constraints on the scatter parameter. Tightening the constraints on the scatter parameter can lead to more precise inference of the central assembly bias parameter.

As shown in Table 5.1, our constraints on the underlying standard HOD model obtained from the model with assembly bias and the model without assembly bias are in good agreement. The only cases in which there are mild tensions between the constraints found from the two models on the underlying HOD parameters, are the  $M_r < -20$  and the  $M_r < -20.5$  samples. However, these tensions are still within one-sigma level. For instance, Figure 8 shows that in the  $M_r < -20.5$  sample, the constraint on the parameter  $\alpha$  found from the model without assembly bias favor slightly higher values than the constraint found from the model with assembly bias. Also the scatter parameter  $\sigma_{\log M}$  is more tightly constrained in the standard HOD model. However, it is important to emphasize that these constraints are still in agreement with each other within a one-sigma level.

Zentner et al. (2014) shows that in the mock catalogs that exhibit significant levels of assembly bias, using a simple mass-only occupation model can lead to considerable biases in inference of the galaxy–halo connection parameters. Although we cannot rule out moderate levels of assembly bias in our findings, we do not find any considerable discrepancy between the two models in terms of estimating the underlying HOD parameters.

A few galaxy–halo connection methods have been proposed in the literature that give rise to assembly bias in the galaxy population. Zentner et al. (2014) demonstrates that the abundance matching techniques based on  $V_{\max}$  (as introduced in Hearin & Watson 2013; Reddick et al. 2013) exhibit some levels of assembly bias. We aim to provide a comparison between the impact of assembly bias on clustering in these mock catalogs and the mock catalogs predicted from our constraints on the decorated HOD model for  $L_*$ -type galaxies. In particular, we consider the abundance matching catalogs produced by Hearin & Watson (2013). These catalogs have been extensively studied for examining potential systematic effects of galaxy assembly bias on cosmological (McEwen & Weinberg 2016) and halo occupation (Zentner et al. 2014) parameter inferences.

This abundance matching catalog was built based on the Bolshoi  $N$ -body simulation (Klypin et al. 2011) using the adaptive refinement tree code (ART Kravtsov et al. 1997). The Box size for this simulation is  $250 h^{-1}\text{Mpc}$ , the number of simulation particles is  $2048^3$ , the mass per simulation particle  $m_p$  is  $1.35 \times 10^8 h^{-1}M_\odot$ , and the gravitational softening length  $\epsilon$  is  $1 h^{-1}\text{kpc}$ . The halos and subhalos in this simulation are identified using the ROCKSTAR

algorithm (Behroozi et al. 2013b). The Hearin & Watson 2013 catalogs make use of  $V_{\text{peak}}$  (maximum  $V_{\text{max}}$  throughout the assembly history of halo) as the subhalo property to be matched to galaxy luminosity.

As noted by Zentner et al. (2014) and McEwen & Weinberg (2016), these galaxy mock catalogs show significant levels of assembly bias in the central galaxy population. This has been demonstrated by investigating the difference in  $w_p$  between the randomized mock catalogs and the original mock catalogs. Randomization is performed in a procedure described in Zentner et al. (2014) which we briefly summarize here: First, halos are divided into different bins of halo mass with width of 0.1 dex. Then all central galaxies are shuffled among all halos within each bin. Once the centrals have been shuffled, within each bin, the satellite systems are shuffled among all halos in that mass bin, preserving their relative distance to the center of halo. This procedure preserves the HOD, but erases any dependence of the galaxy population on the assembly history of halos. Therefore, assembly bias is erased in the randomized galaxy catalog.

For  $L_*$  galaxies, the difference in  $w_p$  between the randomized and the original catalogs of Hearin & Watson (2013) is shown in Figure 4 with the red curves. As demonstrated in Figure 4 (and as previously noted by Zentner et al. 2014; McEwen & Weinberg 2016), the relative difference in  $w_p$  is only significant in relatively large scales ( $r_p > 1\text{Mpc } h^{-1}$ ). This implies that in these catalogs, only the central occupation is affected by assembly bias. This is in agreement with our findings.

Furthermore, we investigate whether the impact of assembly bias on galaxy clustering predicted by our findings are in agreement with the abundance matching catalogs of Hearin & Watson (2013). First, we make random draws from the posterior probability distribution function over the parameters of the model with assembly bias. Then, we create mock catalogs with these random draws, and then we compute the difference in  $w_p$  between the randomized catalogs and the original catalogs. The relative difference in  $w_p$  predicted from our constraints are shown with blue curves in Figure 4.

We note that our findings follow the same trend. That is, we see negligible difference in the small scale clustering and more considerable differences in  $w_p$  on larger scales ( $r_p > 1\text{ Mpc } h^{-1}$ ). Similar to findings of Zentner et al. (2014), Lehmann et al. (2015), and McEwen & Weinberg (2016), we see that the impact of assembly bias on galaxy clustering becomes less significant in brighter galaxy samples. Furthermore, we notice that our mock catalogs favor more moderate changes in galaxy clustering as a result of assembly bias.

## 5.2. model comparison

We want to address this question that whether the constraints on the model with assembly bias and the model without assembly bias given the galaxy clustering data lead us to claim that assembly bias is strongly supported by the observations or not. Within the standard HOD framework, the distribution of the galaxies is modeled using a simple description based on the *mass*-only ansatz:  $P(N|M)$ . The decorated HOD model however, provides a more complex description of the data by adding a secondary halo property (halo concentration in this study) and a more flexible occupation model:  $P(N|M, c)$ .

In order to investigate whether the higher level of model complexity is demanded by the observations or not, we present model comparison between the models with and without assembly bias. In particular, we make use of two simple methods for model comparison: *Akaike Information Criterion* (AIC, [Akaike 1974](#), see [Gelman et al. 2014](#) for detailed discussion on AIC), and *Bayesian Information Criteria* (BIC, [Schwarz 1978](#)). BIC and AIC are more computationally tractable than alternatives approaches such as computing the fully marginalized likelihood. The underlying assumption of these information criteria is that models that yield higher likelihoods are more preferable, but at the same time, models with more flexibility are penalized.

Suppose that  $\mathcal{L}^*$  is the maximum likelihood achieved by the model,  $N_{\text{par}}$  is the number of free parameters in the model, and  $N_{\text{data}}$  is the number of data points in the data set. Then we have

$$\text{BIC} = -2 \ln \mathcal{L}^* + N_{\text{par}} \ln N_{\text{data}} , \quad (15)$$

$$\text{AIC} = -2 \ln \mathcal{L}^* + 2N_{\text{par}} . \quad (16)$$

Given a data set, models with lower value of AIC and BIC are more desired. That is, in order for the higher model complexity (given by  $N_{\text{par}}$ ) to be justified,  $\mathcal{L}^*$  must be sufficiently higher. Therefore in this formulation, models that deliver lower information criteria scores are more preferable.

Figure 5 shows the comparison between the BIC and AIC scores for the model with assembly bias and the model without assembly bias. We note that the model without assembly bias is still preferable by the galaxy clustering observations. That is, although some improvements to fitting the clustering data can be achieved as a result of using a more complicated occupation model, these improvements are not significant enough to justify the use of a more complicated model that takes assembly bias into account.

We note that both AIC and BIC scores improve in the luminosity-threshold samples for which, we have tighter constraints over the central assembly bias parameter. In particular, the model with assembly bias deliver *only slightly* lower AIC scores for the  $M_r < -18, -20$  samples. This supports our intuition that AIC and BIC penalize unconstrained parameters. Also note that, the difference between both BIC and AIC scores are marginal.

### 5.3. choice of simulation

Given the SDSS clustering measurements described in Section 3, We repeat the inference of the assembly bias parameters  $\mathcal{A}_{\text{sat}}$  and  $\mathcal{A}_{\text{cen}}$  with the **BolshoiP** simulation (Klypin et al. 2016). This  $N$ -body simulation is carried out with similar setting as the **Bolshoi** simulation with the exception that in the **BolshoiP** simulation, Planck cosmology is adapted and the mass per simulation particle is  $1.49 \times 10^8 h^{-1} M_{\odot}$ .

The summary of constraints are shown in Figure 6. In Figure 6, the constraints from the **SMDP** and the **BolshoiP** simulations are shown with circles and crosses respectively. Additionally, the upper and lower bounds on the inferred parameters reported by Zentner et al. (2016) are shown in shaded blue regions. In the case of central assembly bias, all three constraints are consistent. For the luminosity-thresholds samples  $M_r < -20.5, -20, -19.5$ , where the central assembly bias parameters are strongly positive, the constraints obtained from the **SMDP** simulation are tighter.

In the case of the satellite assembly bias parameters however, constraints from the **BolshoiP** simulation for the luminosity threshold samples  $M_r < -20.5, -19$  favor more positive values of the parameter, while our constraints from the **SMDP** simulation for these two luminosity thresholds favor zero satellite assembly bias. As it is shown in the lower panel of Figure 6, our constraints from the **BolshoiP** simulations for the  $M_r < -21, -20.5, -20, -19.5, -19$  samples are consistent with the lower and upper bounds (shown with the shaded blue region) reported by Zentner et al. (2016) that uses the same simulation but different  $w_p$  measurements (Zehavi et al. 2011). Therefore, there is some discrepancy between our  $\mathcal{A}_{\text{sat}}$  constraints using the **SMDP** simulation and the **BolshoiP** simulations.

For the  $M_r < -19, -20.5$  samples, the marginalized posterior PDFs over  $\mathcal{A}_{\text{sat}}$  from the two simulations are shown in Figure 7. Note that  $\mathcal{A}_{\text{sat}}$  is poorly constrained in both simulations and for both luminosity-threshold samples. For the  $M_r < -19$  sample, considering how poorly constrained the parameters are, the discrepancy between the constraints is not very stark. Note that the tension is still at a one-sigma level. The discrepancy however, becomes more pronounced in the  $M_r < -20.5$  sample.

In terms of the effect of assembly bias on galaxy clustering, note that mocks created using the inferred parameters with the **SMDP** simulation show the same behavior as we observe in the abundance matching catalogs presented in [Zentner et al. \(2014\)](#) and [Lehmann et al. \(2015\)](#). That is, the difference in  $w_p$  between the mock catalogs and the randomized catalogs is mostly on large scales where the clustering is governed by the central galaxies. That is, the impact of assembly bias on the satellite occupation is negligible and only the central occupation is affected.

## 6. Summary and Conclusion

In this investigation, we provide constraints on the concentration-dependence of halo occupation for a wide range of galaxy luminosities in the SDSS data. In particular, the modeling is done in the context of the decorated HOD model [Hearin et al. \(2016b\)](#), and the data used in this investigation is the projected 2PCF measurements published by [Guo et al. \(2015b\)](#). We make use of **SMDP** high resolution  $N$ -body simulation that enables us to reliably perform inference for the faintest galaxy samples in the SDSS DR7 catalog that live in low mass halos, and the brightest galaxy samples that occupy large comoving volumes.

Our findings suggest that the satellite assembly bias remains consistent with zero. However, our constraints on the central assembly bias parameter exhibit a trend with the luminosity limits of the galaxy samples. For the brightest samples, central assembly bias is consistent with zero, which is in agreement with this picture that the halo assembly bias becomes negligible for the most massive halos.

For the  $M_r < -20.5, -20, -19.5$  samples, at a fixed halo mass, we find positive correlation between the central population and halo concentration at fixed halo mass. For  $M_r < -19, -18.5$  we find no correlation, and for the faintest sample, we find negative correlation. Given the large scale halo assembly bias and the scale-dependent feature of assembly bias in the quasi-linear scales, our constraints on the more flexible HOD model lead to improvement in modeling the galaxy clustering. However, we do not find these improvements to be sufficient to lower the information criteria scores associated with the more complex model. The exceptions are the  $M_r < -20, -18$  luminosity-threshold samples for which we find the strongest constraints on the central assembly bias. For these two samples, the HOD model with assembly bias yields lower BIC score than the model without assembly bias.

We compare the impact of assembly bias on galaxy clustering between the catalogs constructed from our results and the abundance matching catalogs presented in [Hearin & Watson \(2013\)](#); [Zentner et al. \(2014\)](#). We demonstrate that the effect of assembly bias on

galaxy clustering predicted from our results is similar to (but more moderate than) the effects seen in the abundance matching catalogs of [Hearin & Watson \(2013\)](#). That is, assembly bias mostly affects the large scales and the quasi-linear clustering and the small scale clustering remains unaltered. In addition, the effect of assembly bias on galaxy clustering vanishes in the brightest galaxy samples.

Moreover, we repeat our inference using the **BolshoiP** simulation. We find that our findings based on the **BolshoiP** simulation are consistent with constraints reported by [Zentner et al. \(2016\)](#) (in the  $M_r < -21, -20.5, -20, -19.5, -19$  luminosity-threshold samples) that predicts positive satellite assembly bias (correlation between the expected number of satellites and  $V_{\max}$  at fixed host halo mass) for the  $M_r < -19, -20.5$  samples. However, we note that the results based on the **SMDP** simulation are more consistent with the picture provided by the previous models based on the abundance matching technique (e.g. [Zentner et al. 2014](#); [Lehmann et al. 2015](#)). That is, only the large-scale clustering, governed by the centrals, is affected by assembly bias.

## Acknowledgments

We are grateful to David W. Hogg, Alex I. Malz, Andrew Hearin, Andrew Zentner, Chia-Hsun Chuang, Michael R. Blanton, and Kilian Walsh for discussions related to this work. This work was supported by the NSF grant AST-1517237. All the computations in this work were carried out in the New York University High Performance Computing Mercer facility. We thank Shenglong Wang, the administrator of the NYU HPC center for his continuous and consistent support throughout the completion of this study.

The CosmoSim database used in this paper is a service by the Leibniz-Institute for Astrophysics Potsdam (AIP). The MultiDark database was developed in cooperation with the Spanish MultiDark Consolider Project CSD2009-00064. The authors gratefully acknowledge the Gauss Centre for Supercomputing e.V. ([www.gauss-centre.eu](http://www.gauss-centre.eu)) and the Partnership for Advanced Supercomputing in Europe (PRACE, [www.prace-ri.eu](http://www.prace-ri.eu)) for funding the MultiDark simulation project by providing computing time on the GCS Supercomputer SuperMUC at Leibniz Supercomputing Centre (LRZ, [www.lrz.de](http://www.lrz.de)).

All of the code written for this project is available in an open-source code repository at <https://github.com/mjvakili/gambly>. The SDSS clustering measurements and the covariance matrices used in this work are available at [http://sdss4.shao.ac.cn/guoh/files/wpxi\\_measurements\\_Guo15.tar.gz](http://sdss4.shao.ac.cn/guoh/files/wpxi_measurements_Guo15.tar.gz). Description of the **SMDP** and the **BolshoiP** halo catalogs used in this investigation can be found at <https://www.cosmosim.org/cms/>

**simulations.** The RockStar halo catalogs of the SMDP and the BolshoiP simulations are publicly available at <http://yun.ucsc.edu/sims/SMDPL/hlists/index.html> and [http://yun.ucsc.edu/sims/Bolshoi\\_Planck/hlists/index.html](http://yun.ucsc.edu/sims/Bolshoi_Planck/hlists/index.html) respectively. We thank Peter Behroozi for making the halo catalogs publicly available. In this work we have made use of the publicly available codes: corner (Foreman-Mackey 2016), emcee (Foreman-Mackey et al. 2013), halotools (Hearin et al. 2016a), Corrfunc (Sinha 2016), and changtools (<https://github.com/changhoonhahn/ChangTools>). The abundance matching mock catalogs used in this study are available at (<http://logrus.uchicago.edu/~aphearin/>).



Table 1: **Prior Specifications:** The prior probability distribution and its range for each of the parameters. All mass parameters are in unit of  $h^{-1}M_{\odot}$ . The parameters marked by \* are only used in the Heaviside Assembly bias modeling and by definition are bounded between -1 and 1.

Parameter	Prior	Range
$\alpha$	Uniform	[0.85, 1.45]
$\sigma_{\log M}$	Uniform	[0.05, 1.5]
$\log M_0$	Uniform	[10.0, 14.5]
$\log M_{\min}$	Uniform	[10.0, 14.0]
$\log M_1$	Uniform	[11.5, 15.0]
$\mathcal{A}_{\text{cen}}^*$	Uniform	[-1.0, 1.0]
$\mathcal{A}_{\text{sat}}^*$	Uniform	[-1.0, 1.0]

Table 2: **Constraints:** Constraints on the parameters of the HOD models with and without assembly bias. All mass parameters are in unit of  $h^{-1}M_{\odot}$ . The best-estimates and the error bars correspond to the 50% quantile and 68% confidence intervals obtained from the marginalized posterior probability pdfs. The last column is  $\chi^2$  per degrees of freedom (*dof*), where  $dof = N_{data} - N_{par}$

$M_{r,lim}$	$\log M_{min}$	$\sigma_{\log M}$	$\log M_0$	$\alpha$	$\log M_1$	$\mathcal{A}_{cen}$	$\mathcal{A}_{sat}$	$\chi^2/dof$
-18	$11.56^{+0.21}_{-0.25}$	$1.05^{+0.31}_{-0.52}$	$10.84^{+0.77}_{-0.59}$	$0.98^{+0.05}_{-0.05}$	$12.50^{+0.10}_{-0.10}$	—	—	14.51/8
-18	$11.53^{+0.23}_{-0.21}$	$1.08^{+0.28}_{-0.51}$	$10.86^{+0.81}_{-0.62}$	$0.97^{+0.05}_{-0.04}$	$12.56^{+0.09}_{-0.10}$	$-0.67^{+0.55}_{-0.25}$	$-0.30^{+1.09}_{-0.54}$	7.52/6
-18.5	$11.67^{+0.29}_{-0.25}$	$0.83^{+0.45}_{-0.53}$	$10.85^{+0.64}_{-0.60}$	$1.02^{+0.04}_{-0.04}$	$12.69^{+0.08}_{-0.08}$	—	—	6.17/8
-18.5	$11.60^{+0.31}_{-0.20}$	$0.74^{+0.49}_{-0.46}$	$10.73^{+0.69}_{-0.51}$	$1.01^{+0.05}_{-0.05}$	$12.72^{+0.09}_{-0.10}$	$0.02^{+0.67}_{-0.62}$	$0.07^{+0.53}_{-0.59}$	6.23/6
-19	$11.74^{+0.37}_{-0.18}$	$0.62^{+0.52}_{-0.39}$	$10.82^{+0.62}_{-0.56}$	$1.04^{+0.04}_{-0.04}$	$12.87^{+0.09}_{-0.09}$	—	—	8.69/8
-19	$11.71^{+0.37}_{-0.16}$	$0.58^{+0.53}_{-0.38}$	$10.75^{+0.66}_{-0.52}$	$1.03^{+0.04}_{-0.05}$	$12.90^{+0.10}_{-0.09}$	$0.36^{+0.44}_{-0.62}$	$-0.01^{+0.56}_{-0.54}$	8.87/6
-19.5	$11.78^{+0.37}_{-0.13}$	$0.51^{+0.53}_{-0.31}$	$11.09^{+0.69}_{-0.73}$	$1.06^{+0.03}_{-0.04}$	$13.03^{+0.08}_{-0.07}$	—	—	6.80/8
-19.5	$11.82^{+0.41}_{-0.17}$	$0.62^{+0.54}_{-0.44}$	$11.11^{+0.68}_{-0.77}$	$1.03^{+0.04}_{-0.06}$	$13.03^{+0.10}_{-0.08}$	$0.52^{+0.32}_{-0.47}$	$-0.01^{+0.66}_{-0.49}$	5.56/6
-20	$12.01^{+0.17}_{-0.08}$	$0.32^{+0.32}_{-0.19}$	$11.69^{+0.54}_{-0.99}$	$1.08^{+0.03}_{-0.05}$	$13.32^{+0.08}_{-0.07}$	—	—	13.45/8
-20	$12.23^{+0.39}_{-0.24}$	$0.76^{+0.41}_{-0.43}$	$11.66^{+0.62}_{-0.94}$	$1.00^{+0.08}_{-0.05}$	$13.26^{+0.08}_{-0.09}$	$0.81^{+0.12}_{-0.26}$	$-0.15^{+0.33}_{-0.31}$	8.12/6
-20.5	$12.31^{+0.06}_{-0.06}$	$0.21^{+0.14}_{-0.11}$	$12.36^{+0.27}_{-0.77}$	$1.11^{+0.08}_{-0.08}$	$13.56^{+0.09}_{-0.09}$	—	—	11.40/8
-20.5	$12.37^{+0.16}_{-0.09}$	$0.44^{+0.28}_{-0.26}$	$12.38^{+0.27}_{-0.54}$	$1.05^{+0.08}_{-0.07}$	$13.60^{+0.10}_{-0.08}$	$0.81^{+0.15}_{-0.43}$	$-0.11^{+0.26}_{-0.27}$	6.82/6
-21	$12.73^{+0.14}_{-0.07}$	$0.32^{+0.22}_{-0.17}$	$12.62^{+0.48}_{-1.36}$	$1.17^{+0.10}_{-0.16}$	$14.01^{+0.08}_{-0.10}$	—	—	7.34/8
-21	$12.81^{+0.28}_{-0.11}$	$0.47^{+0.41}_{-0.25}$	$12.51^{+0.61}_{-1.17}$	$1.08^{+0.17}_{-0.13}$	$14.02^{+0.08}_{-0.10}$	$0.33^{+0.51}_{-0.64}$	$-0.18^{+0.41}_{-0.35}$	7.21/6
-21.5	$13.44^{+0.11}_{-0.09}$	$0.60^{+0.09}_{-0.11}$	$12.57^{+0.77}_{-1.27}$	$1.33^{+0.07}_{-0.21}$	$14.53^{+0.05}_{-0.07}$	—	—	3.29/8
-21.5	$13.43^{+0.12}_{-0.06}$	$0.60^{+0.12}_{-0.08}$	$12.59^{+0.64}_{-1.25}$	$1.27^{+0.11}_{-0.19}$	$14.54^{+0.05}_{-0.05}$	$-0.24^{+0.50}_{-0.40}$	$-0.30^{+0.86}_{-0.49}$	3.37/6

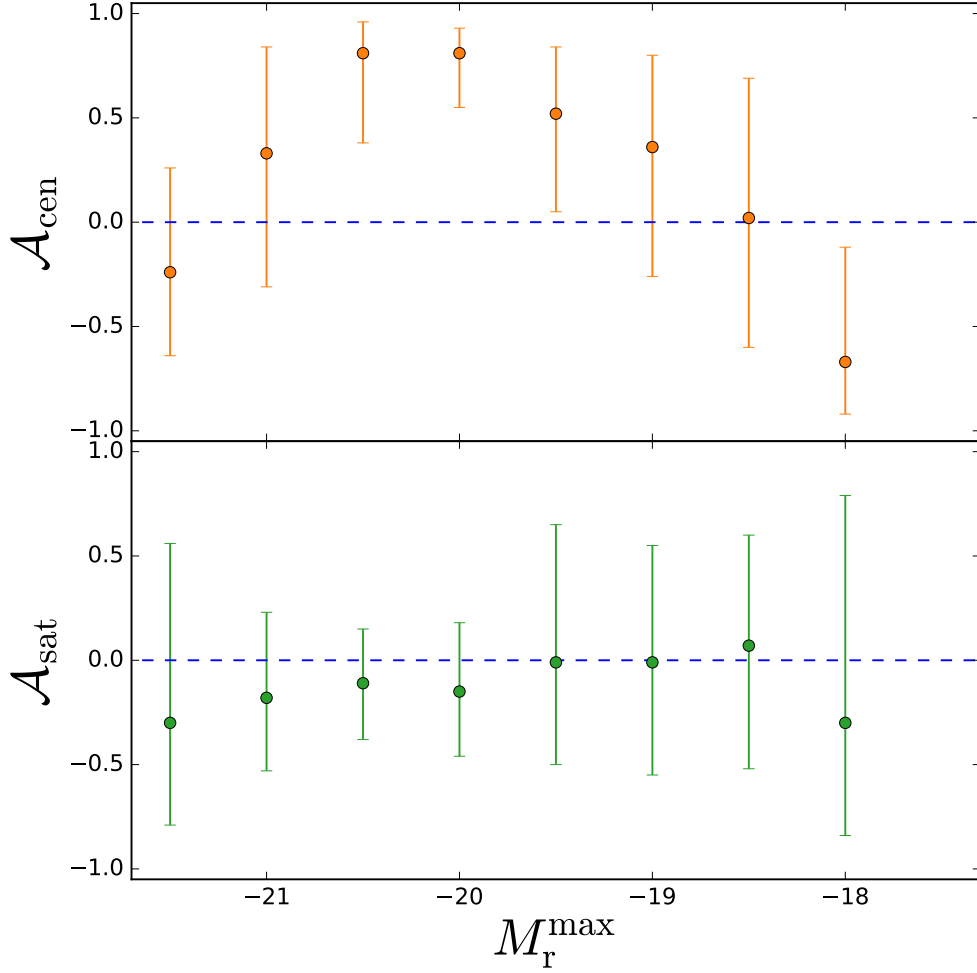


Fig. 1.— Constraints on the central assembly bias  $\mathcal{A}_{\text{cen}}$  (Top panel) and the satellite assembly bias  $\mathcal{A}_{\text{sat}}$  (Bottom panel) parameters. The  $\mathcal{A}_{\text{cen}}$  constraints for the  $M_r < -20.5$ ,  $-20$ ,  $-19.5$  samples favor positive values of  $\mathcal{A}_{\text{cen}}$  with the tightest constraint coming from the  $M_r < -20$  sample. The  $\mathcal{A}_{\text{cen}}$  constraints for the  $M_r < -18$  sample favor negative values of  $\mathcal{A}_{\text{cen}}$ . All the  $\mathcal{A}_{\text{sat}}$  constraints are consistent with no satellite assembly bias.

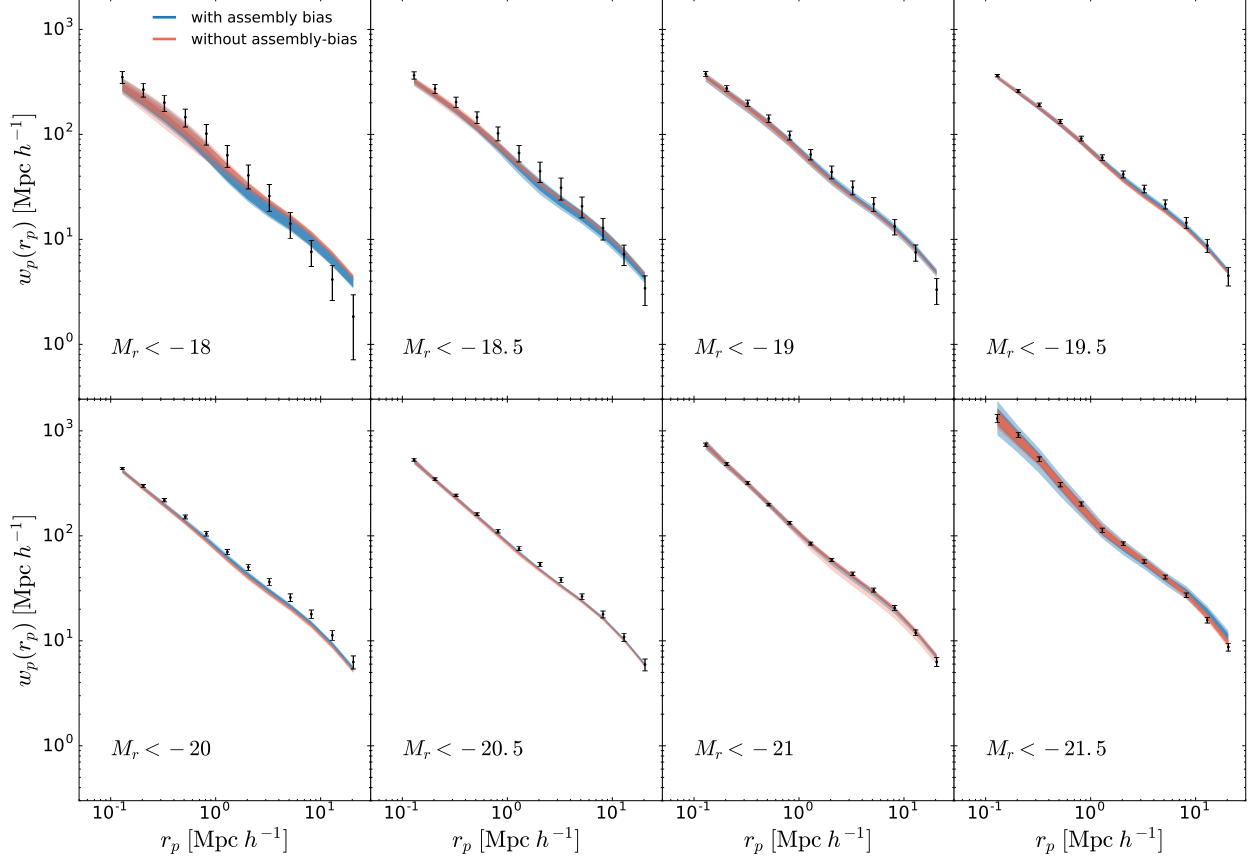


Fig. 2.— Comparison between the posterior predictions of  $w_p(r_p)$  and the SDSS  $w_p(r_p)$  measurements. Predictions from the standard HOD model (HOD model with assembly bias) are shown in red (blue). The Dark and light shaded regions mark the 68% and the 95% confidence intervals. The errorbars are from the diagonal elements of the covariance matrix.

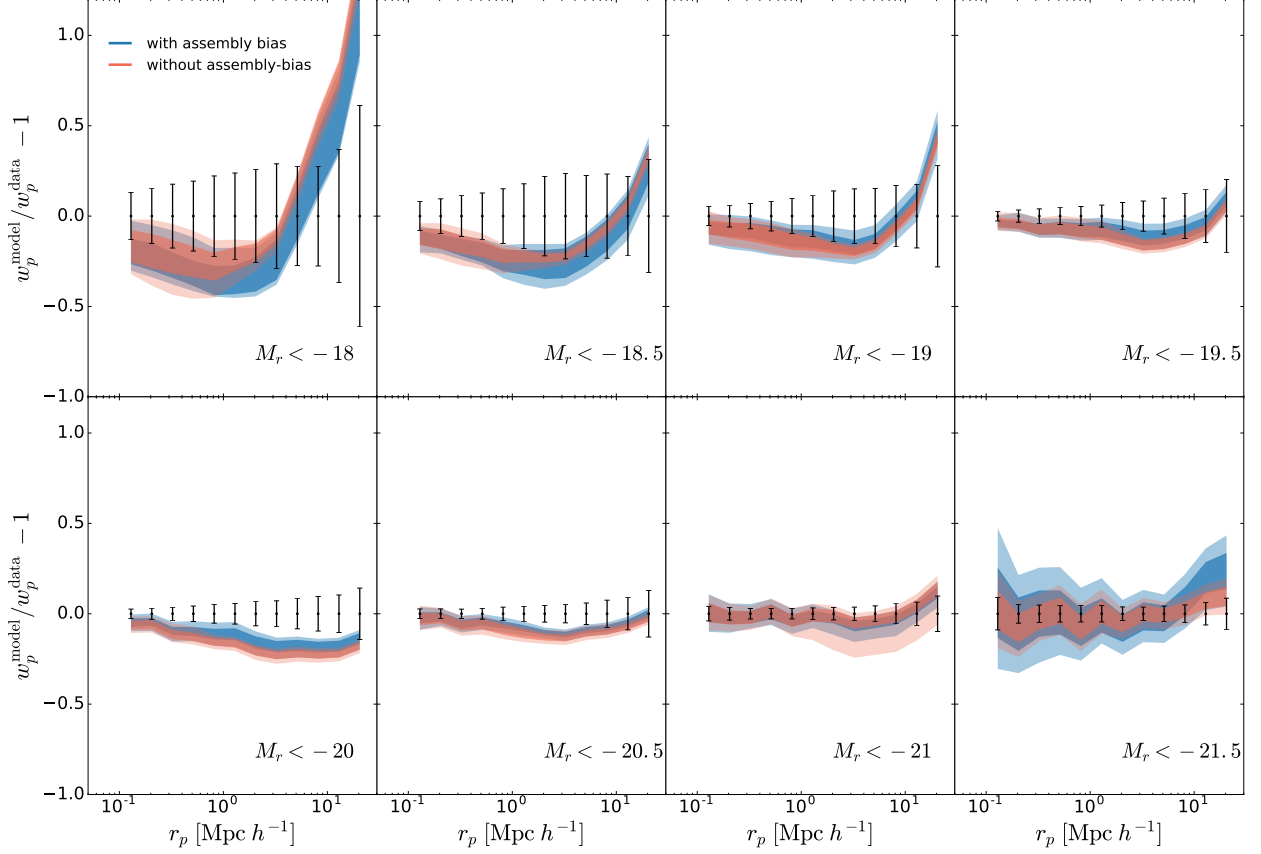


Fig. 3.— Same as Figure 2, but showing the fractional difference between the posterior predictions and the observed projected 2PCF for all the luminosity threshold samples. In all luminosity threshold samples, predictions of the two models for small scale clustering are consistent. In the samples that favor more positive values of the central assembly bias parameter ( $M_r < -19.5, -19, -20, -20.5$ ), modeling of the intermediate and large scale clustering is slightly improved. The large scale clustering modeling of the  $M_r < -18$  sample is also improved because of negative constraints on  $\mathcal{A}_{\text{cen}}$  which is equivalent to allocation of more central galaxies in low concentration halos at fixed halo mass.

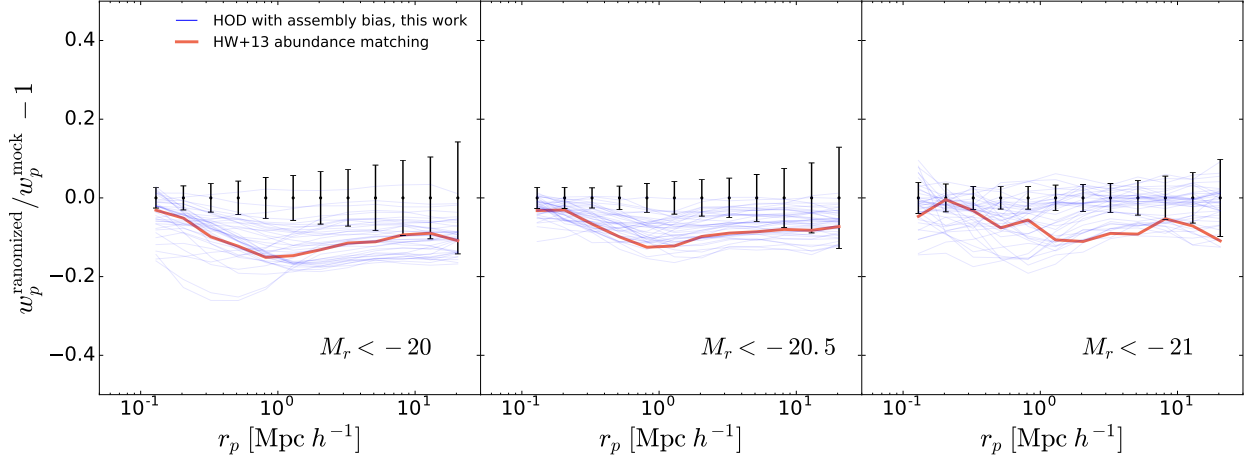


Fig. 4.— Demonstration of the relative difference in  $w_p$  between randomized and non-randomized catalogs for different luminosity threshold samples:  $M_r < -20, -20.5, -21$ . The errorbars are from the diagonal elements of the covariance matrix. The blue lines correspond to the random draws from the posterior probability (summarized in Table 5.1) over the parameters of the HOD model with assembly bias. The red line corresponds to the subhalo abundance matching catalog (Hearin & Watson 2013; Hearin et al. 2014). Our constraints favor *more moderate* levels of the impact of assembly bias on galaxy clustering than the levels seen in the abundance matching mock catalogs. Within both models, the small scale clustering remains unaltered after randomizing the catalogs, signaling the lack of correlation between the satellite occupation and the halo concentration at a fixed mass in the two models.

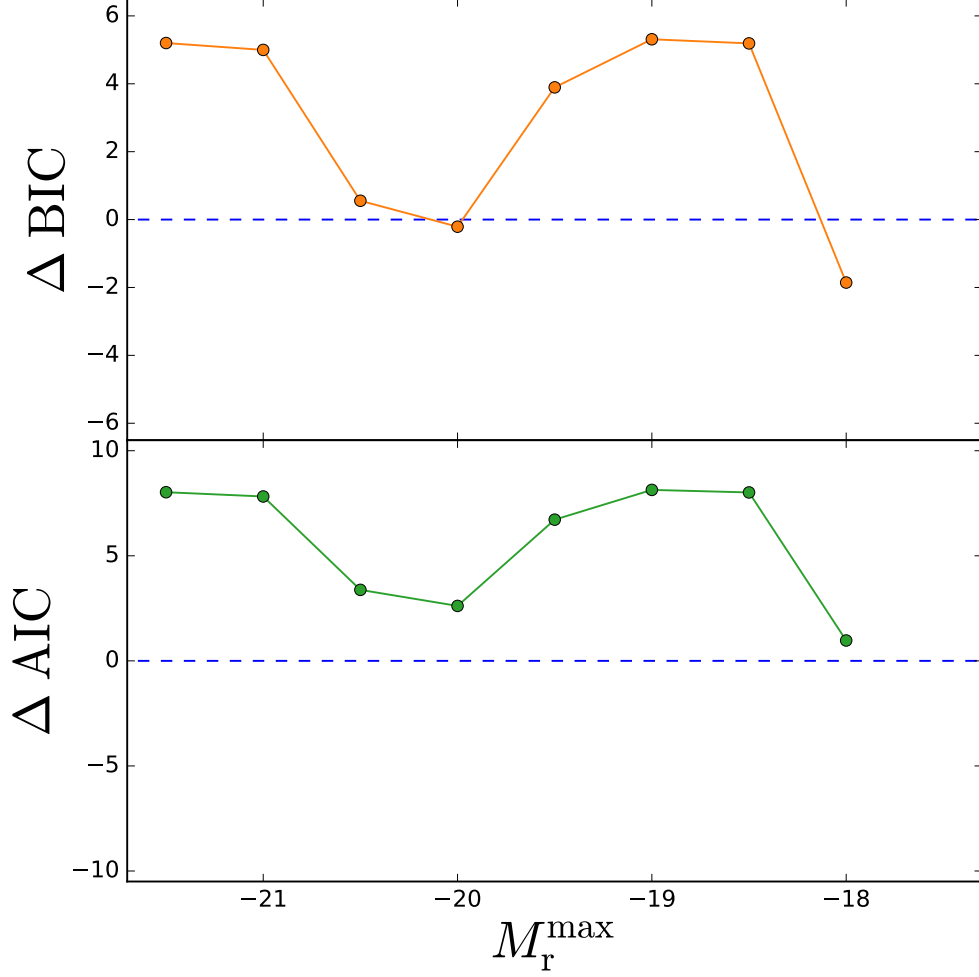


Fig. 5.— Difference in the information criteria between the HOD model with assembly bias and the model without assembly bias. **Top:**  $\Delta BIC = BIC(\text{with assembly bias}) - BIC(\text{without assembly bias})$ . **Bottom:**  $\Delta AIC = AIC(\text{with assembly bias}) - AIC(\text{without assembly bias})$ . According to BIC (AIC), the more complex model with assembly bias is favored once  $\Delta BIC < 0$  ( $\Delta AIC < 0$ ). Both  $\Delta BIC$  and  $\Delta AIC$  are lower for the samples with tighter constraints over the central assembly bias parameter  $\mathcal{A}_{\text{cen}}$ , with  $\Delta BIC$  being (marginally) negative only for  $M_r < -20$ ,  $-18$  samples that yield strongest constraints on  $\mathcal{A}_{\text{cen}}$ .



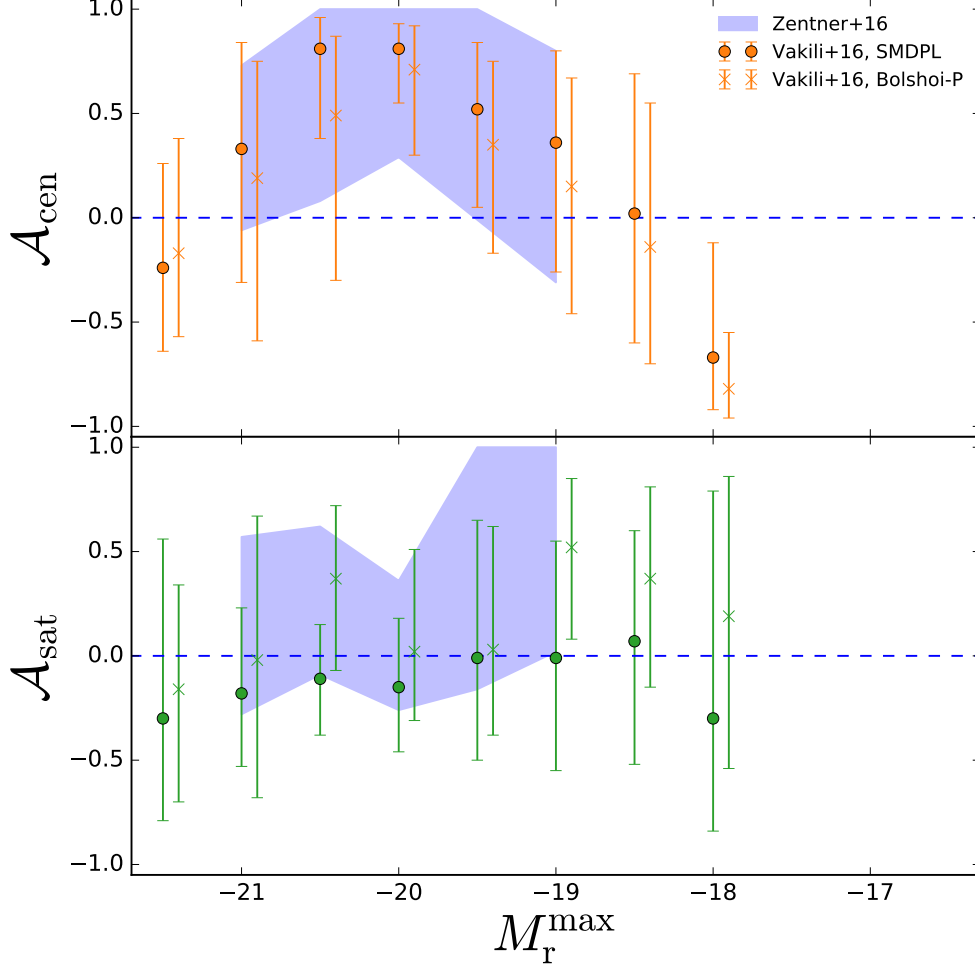


Fig. 6.— Comparison between the constraints on the assembly bias parameters  $\mathcal{A}_{\text{cen}}$  (shown in the top panel) and  $\mathcal{A}_{\text{sat}}$  (shown in the bottom panel) for different simulations: **SMDP** (shown with circle), and **BolshoiP** (shown with cross). The errorbars mark the 68% uncertainty over the parameters. Shaded blue regions show the upper and lower bounds reported by [Zentner et al. \(2016\)](#) that uses the **BolshoiP** and clustering measurements of [Zehavi et al. \(2011\)](#). For the confidence intervals corresponding to the shaded blue regions, we refer the readers to Table 2 of [Zentner et al. \(2016\)](#). The central assembly bias constraints found from the two simulations are consistent, with the constraints for from the **SMDP** simulation being tighter for the most luminous samples. The constraints on  $\mathcal{A}_{\text{sat}}$  from the two simulations are largely in agreement with the exception of  $M_{\text{r}} < -19$ ,  $-20.5$  samples that favor more positive values of  $\mathcal{A}_{\text{sat}}$  when the **BolshoiP** simulation is used.

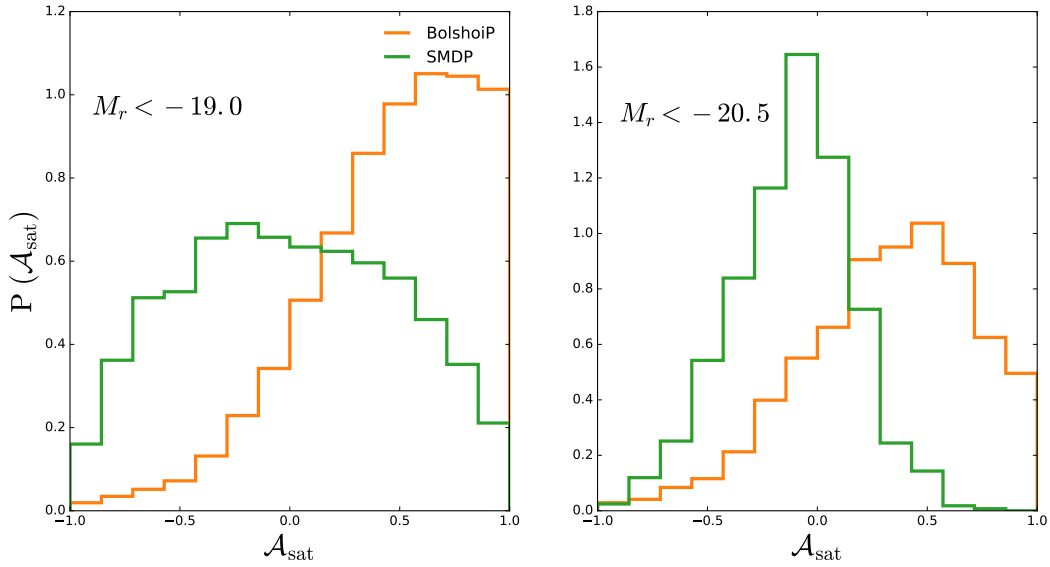


Fig. 7.— Constraints over the satellite assembly bias parameters from luminosity-threshold samples  $M_r < -19$ ,  $-20.5$ , for two different simulations: BolshoiP (yellow), and SMDPL (green). The  $\mathcal{A}_{\text{sat}}$  constraints found using the BolshoiP simulation favor more positive values of  $\mathcal{A}_{\text{sat}}$ , while the constraints found using the SMDP simulation favor zero satellite assembly bias.

## REFERENCES

- Abazajian, K., Zheng, Z., Zehavi, I., et al. 2005, *ApJ*, 625, 613
- Abazajian, K. N., Adelman-McCarthy, J. K., Agüeros, M. A., et al. 2009, *ApJS*, 182, 543
- Akaike, H. 1974, *IEEE Transactions on Automatic Control*, 19, 716
- Angulo, R. E., Baugh, C. M., & Lacey, C. G. 2008, *MNRAS*, 387, 921
- Behroozi, P. S., Wechsler, R. H., & Conroy, C. 2013a, *ApJ*, 770, 57
- Behroozi, P. S., Wechsler, R. H., & Wu, H.-Y. 2013b, *ApJ*, 762, 109
- Berlind, A. A., & Weinberg, D. H. 2002, *ApJ*, 575, 587
- Blanton, M. R., Hogg, D. W., Bahcall, N. A., et al. 2003, *ApJ*, 592, 819
- Blanton, M. R., Schlegel, D. J., Strauss, M. A., et al. 2005, *AJ*, 129, 2562
- Cacciato, M., van den Bosch, F. C., More, S., Mo, H., & Yang, X. 2013, *MNRAS*, 430, 767
- Chaves-Montero, J., Angulo, R. E., Schaye, J., et al. 2016, *MNRAS*, arXiv:1507.01948
- Conroy, C., & Wechsler, R. H. 2009, *ApJ*, 696, 620
- Coupon, J., Arnouts, S., van Waerbeke, L., et al. 2015, *MNRAS*, 449, 1352
- Croton, D. J., Gao, L., & White, S. D. M. 2007, *MNRAS*, 374, 1303
- Dalal, N., White, M., Bond, J. R., & Shirokov, A. 2008, *ApJ*, 687, 12
- Dawson, K. S., Schlegel, D. J., Ahn, C. P., et al. 2013, *AJ*, 145, 10
- Dutton, A. A., & Macciò, A. V. 2014, *MNRAS*, 441, 3359
- Foreman-Mackey, D. 2016, *The Journal of Open Source Software*, 24, doi:10.21105/joss.00024
- Foreman-Mackey, D., Hogg, D. W., Lang, D., & Goodman, J. 2013, *PASP*, 125, 306
- Gao, L., Springel, V., & White, S. D. M. 2005, *MNRAS*, 363, L66
- Gao, L., & White, S. D. M. 2007, *MNRAS*, 377, L5
- Gelman, A., Hwang, J., & Vehtari, A. 2014, *Statistics and Computing*, 24, 997
- Gelman, A., & Rubin, D. B. 1992, *Statistical science*, 457

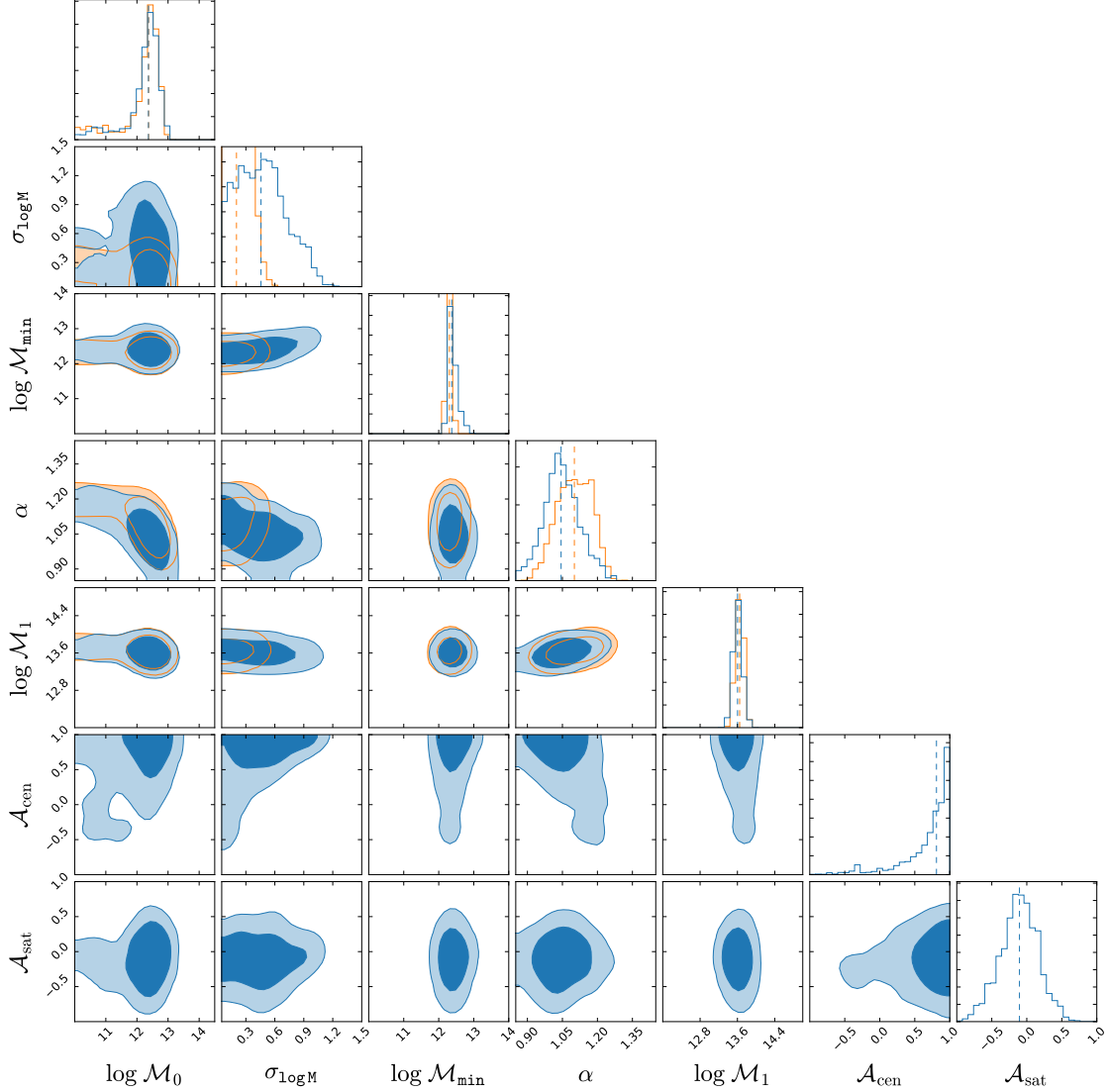


Fig. 8.— An example of posterior probability distribution over the parameters of the standard HOD model with no assembly bias (shown with yellow), and the HOD model with assembly bias (shown in blue). These constraints are obtained from the clustering measurements of the  $M_r < -20.5$  luminosity threshold sample. The dark (light) blue shaded regions show the 68% (95 %) confidence intervals. The constraints on  $\mathcal{A}_{\text{cen}}$  and  $\mathcal{A}_{\text{sat}}$  show positive correlation between the central occupation and the halo concentration at fixed halo mass, and lack of correlation between the satellite occupation and halo concentration at fixed halo mass.

- Gil-Marín, H., Jimenez, R., & Verde, L. 2011, MNRAS, 414, 1207
- Goodman, J., & Weare, J. 2010, Communications in applied mathematics and computational science, 5, 65
- Guo, H., Zehavi, I., & Zheng, Z. 2012, ApJ, 756, 127
- Guo, H., Zheng, Z., Jing, Y. P., et al. 2015a, MNRAS, 449, L95
- Guo, H., Zheng, Z., Zehavi, I., et al. 2015b, MNRAS, 453, 4368
- Guo, H., Zheng, Z., Behroozi, P. S., et al. 2016, MNRAS, 459, 3040
- Guo, Q., White, S., Li, C., & Boylan-Kolchin, M. 2010, MNRAS, 404, 1111
- Hahn, C., Vakili, M., Walsh, K., et al. 2016, ArXiv e-prints, arXiv:1607.01782
- Harker, G., Cole, S., Helly, J., Frenk, C., & Jenkins, A. 2006, MNRAS, 367, 1039
- Hartlap, J., Simon, P., & Schneider, P. 2007, A&A, 464, 399
- Hearin, A., Campbell, D., Tollerud, E., et al. 2016a, ArXiv e-prints, arXiv:1606.04106
- Hearin, A. P., & Watson, D. F. 2013, MNRAS, 435, 1313
- Hearin, A. P., Watson, D. F., Becker, M. R., et al. 2014, MNRAS, 444, 729
- Hearin, A. P., Zentner, A. R., Berlind, A. A., & Newman, J. A. 2013, MNRAS, 433, 659
- Hearin, A. P., Zentner, A. R., van den Bosch, F. C., Campbell, D., & Tollerud, E. 2016b, MNRAS, arXiv:1512.03050
- Hudson, M. J., Gillis, B. R., Coupon, J., et al. 2015, MNRAS, 447, 298
- Klypin, A., Yepes, G., Gottlöber, S., Prada, F., & Heß, S. 2016, MNRAS, 457, 4340
- Klypin, A. A., Trujillo-Gomez, S., & Primack, J. 2011, ApJ, 740, 102
- Kravtsov, A. V. 2013, ApJ, 764, L31
- Kravtsov, A. V., Berlind, A. A., Wechsler, R. H., et al. 2004, ApJ, 609, 35
- Kravtsov, A. V., Klypin, A. A., & Khokhlov, A. M. 1997, ApJS, 111, 73
- Leauthaud, A., Tinker, J., Bundy, K., et al. 2012, ApJ, 744, 159

- Lehmann, B. V., Mao, Y.-Y., Becker, M. R., Skillman, S. W., & Wechsler, R. H. 2015, ArXiv e-prints, arXiv:1510.05651
- Li, Y., Mo, H. J., & Gao, L. 2008, MNRAS, 389, 1419
- Manera, M., Scoccimarro, R., Percival, W. J., et al. 2013, MNRAS, 428, 1036
- Mao, Y.-Y., Williamson, M., & Wechsler, R. H. 2015, ApJ, 810, 21
- McEwen, J. E., & Weinberg, D. H. 2016, ArXiv e-prints, arXiv:1601.02693
- Miyatake, H., More, S., Takada, M., et al. 2016, Physical Review Letters, 116, 041301
- Miyatake, H., More, S., Mandelbaum, R., et al. 2015, ApJ, 806, 1
- More, S., Miyatake, H., Mandelbaum, R., et al. 2015, ApJ, 806, 2
- More, S., van den Bosch, F. C., & Cacciato, M. 2009, MNRAS, 392, 917
- More, S., van den Bosch, F. C., Cacciato, M., et al. 2013, MNRAS, 430, 747
- More, S., Miyatake, H., Takada, M., et al. 2016, ArXiv e-prints, arXiv:1601.06063
- Navarro, J. F., Hayashi, E., Power, C., et al. 2004, MNRAS, 349, 1039
- Neistein, E., Weinmann, S. M., Li, C., & Boylan-Kolchin, M. 2011, MNRAS, 414, 1405
- Norberg, P., Baugh, C. M., Gaztañaga, E., & Croton, D. J. 2009, MNRAS, 396, 19
- Parejko, J. K., Sunayama, T., Padmanabhan, N., et al. 2013, MNRAS, 429, 98
- Prada, F., Klypin, A. A., Cuesta, A. J., Betancort-Rijo, J. E., & Primack, J. 2012, MNRAS, 423, 3018
- Reddick, R. M., Wechsler, R. H., Tinker, J. L., & Behroozi, P. S. 2013, ApJ, 771, 30
- Rodríguez-Puebla, A., Behroozi, P., Primack, J., et al. 2016, MNRAS, 462, 893
- Rodríguez-Puebla, A., Drory, N., & Avila-Reese, V. 2012, ApJ, 756, 2
- Schwarz, G. 1978, Annals of Statistics, 6, 461
- Scoccimarro, R., Sheth, R. K., Hui, L., & Jain, B. 2001, ApJ, 546, 20
- Seljak, U. 2000, MNRAS, 318, 203
- Sheth, R. K., & Tormen, G. 2004, MNRAS, 350, 1385

- Sinha, M. 2016, Corrfunc: Corrfunc-1.1.0, doi:10.5281/zenodo.55161
- Sunayama, T., Hearin, A. P., Padmanabhan, N., & Leauthaud, A. 2016, MNRAS, 458, 1510
- Tasitsiomi, A., Kravtsov, A. V., Wechsler, R. H., & Primack, J. R. 2004, ApJ, 614, 533
- Tinker, J., Kravtsov, A. V., Klypin, A., et al. 2008a, ApJ, 688, 709
- Tinker, J. L. 2007, MNRAS, 374, 477
- Tinker, J. L., & Conroy, C. 2009, ApJ, 691, 633
- Tinker, J. L., Conroy, C., Norberg, P., et al. 2008b, ApJ, 686, 53
- Tinker, J. L., Leauthaud, A., Bundy, K., et al. 2013, ApJ, 778, 93
- Tinker, J. L., Robertson, B. E., Kravtsov, A. V., et al. 2010, ApJ, 724, 878
- Tinker, J. L., Weinberg, D. H., & Warren, M. S. 2006, ApJ, 647, 737
- Tinker, J. L., Weinberg, D. H., Zheng, Z., & Zehavi, I. 2005, ApJ, 631, 41
- Tinker, J. L., Sheldon, E. S., Wechsler, R. H., et al. 2012, ApJ, 745, 16
- Vale, A., & Ostriker, J. P. 2004, MNRAS, 353, 189
- van den Bosch, F. C., Jiang, F., Hearin, A., et al. 2014, MNRAS, 445, 1713
- van den Bosch, F. C., Mo, H. J., & Yang, X. 2003, MNRAS, 345, 923
- van den Bosch, F. C., More, S., Cacciato, M., Mo, H., & Yang, X. 2013, MNRAS, 430, 725
- Wang, H. Y., Mo, H. J., & Jing, Y. P. 2007, MNRAS, 375, 633
- Watson, D. F., Berlind, A. A., & Zentner, A. R. 2012, ApJ, 754, 90
- Watson, W. A., Iliev, I. T., D’Aloisio, A., et al. 2013, MNRAS, 433, 1230
- Wechsler, R. H., Zentner, A. R., Bullock, J. S., Kravtsov, A. V., & Allgood, B. 2006, ApJ, 652, 71
- Wetzel, A. R., & White, M. 2010, MNRAS, 403, 1072
- White, M., Tinker, J. L., & McBride, C. K. 2014, MNRAS, 437, 2594
- York, D. G., Adelman, J., Anderson, Jr., J. E., et al. 2000, AJ, 120, 1579



- Zehavi, I., Zheng, Z., Weinberg, D. H., et al. 2011, *ApJ*, 736, 59
- Zentner, A. R., Berlind, A. A., Bullock, J. S., Kravtsov, A. V., & Wechsler, R. H. 2005, *ApJ*, 624, 505
- Zentner, A. R., Hearin, A., van den Bosch, F. C., Lange, J. U., & Villarreal, A. 2016, *ArXiv e-prints*, arXiv:1606.07817
- Zentner, A. R., Hearin, A. P., & van den Bosch, F. C. 2014, *MNRAS*, 443, 3044
- Zheng, Z., Coil, A. L., & Zehavi, I. 2007, *ApJ*, 667, 760
- Zheng, Z., & Guo, H. 2016, *MNRAS*, 458, 4015
- Zheng, Z., Berlind, A. A., Weinberg, D. H., et al. 2005, *ApJ*, 633, 791
- Zu, Y., & Mandelbaum, R. 2015, *MNRAS*, 454, 1161
- . 2016, *MNRAS*, 457, 4360